Acta Biomaterialia 126 (2021) 109–118

Contents lists available at ScienceDirect

Acta Biomaterialia

journal homepage: www.elsevier.com/locate/actbio

Full length article

Angiogenic hydrogels for dental pulp revascularization

Zain Siddiqui[a], Biplab Sarkar[a], Ka-Kyung Kim[a], Nurten Kadincesme[a], Reshma Paul[a], Arjun Kumar[a], Yoshifumi Kobayashi[b], Abhishek Roy[a], Marwa Choudhury[a], Jian Yang[c], Emi Shimizu[b], Vivek A. Kumar[a,b,d,e,*]

[a] Department of Biomedical Engineering, New Jersey Institute of Technology, Newark, NJ, USA
[b] Department of Oral Biology, Department of Endodontics, Rutgers School of Dental Medicine, Newark, NJ, USA
[c] Department of Biomedical Engineering, Huck Institutes of The Life Sciences, Materials Research Institute, Pennsylvania State University, University Park, PA, USA
[d] Department of Chemical and Materials Engineering, New Jersey Institute of Technology, Newark, NJ, USA
[e] Department of Restorative Dentistry, Rutgers School of Dental Medicine, Newark, NJ, USA

ARTICLE INFO

Article history:
Received 7 January 2021
Revised 24 February 2021
Accepted 1 March 2021
Available online 6 March 2021

Keywords:
Self-assembly
Angiogenesis
Acellular scaffolds
Tissue regeneration
Pulp revascularization

ABSTRACT

Angiogenesis is critical for tissue healing and regeneration. Promoting angiogenesis in materials implanted within dental pulp after pulpectomy is a major clinical challenge in endodontics. We demonstrate the ability of acellular self-assembling peptide hydrogels to create extracellular matrix mimetic architectures that guide *in vivo* development of neovasculature and tissue deposition. The hydrogels possess facile injectability, as well as sequence-level functionalizability. We explore the therapeutic utility of an angiogenic hydrogel to regenerate vascularized pulp-like soft tissue in a large animal (canine) orthotopic model. The regenerated soft tissue recapitulates key features of native pulp, such as blood vessels, neural filaments, and an odontoblast-like layer next to dentinal tubules. Our study establishes angiogenic peptide hydrogels as potent scaffolds for promoting soft tissue regeneration *in vivo*.

Statement of Significance

A major challenge to endodontic tissue engineering is the lack of *in situ* angiogenesis within intracanal implants, especially after complete removal of the dental pulp. The lack of a robust vasculature in implants limit integration of matrices with the host tissue and regeneration of soft tissue. We demonstrate the development of an acellular material that promotes tissue revascularization *in vivo* without added growth factors, in a preclinical canine model of pulp-like soft-tissue regeneration. Such acellular biomaterials would facilitate pulp revascularization approaches in large animal models, and translation into human clinical trials.

1. Introduction

In the human body, most cells are within 150 μm of a capillary — due to inherent diffusion limits to the supply of nutrients and oxygen [1]. Unsurprisingly, therapeutic angiogenesis is critical for tissue regeneration [2–4], especially after ischemic tissue damage [5]. Specific vascularization strategies could be clinically relevant for ischemic diseases such as coronary artery disease [6] and critical limb ischemia [7], improving islet transplant tolerability [8], and optimizing vascularization of osteo-conductive implants [9]. Where pre-vascularized/pre-cellularized tissue-engineering strategies are not viable due to lack of oxygen/nutrient supply, *in vivo* vascularization may prove especially valuable [10,11]. Many promising vascularization strategies require cumbersome cell sourcing, or may result in rapid diffusion of bioactive factors from the delivery site with ectopic side effects [3,12]. There remains a significant need for an off-the-shelf material-based alternative that is injectable, biodegradable, and capable of promoting *in situ* neovascularization and matrix deposition — for wider adoption, lower cost and clinical use.

Injectable hydrogels that can assemble to conform to tissue defects *in vivo* can augment and repair injured soft tissues [13]. Optimally, these gels would be injected by a needle or a

* Corresponding author.
E-mail address: vak@njit.edu (V.A. Kumar).

https://doi.org/10.1016/j.actbio.2021.03.001
1742-7061/

Table 1
Comparison of relevant peptides.

Peptide	sequence	format	conformation
SLan *angiogenic*target peptide	$K(SL)_6K$–G–KLTWQELYQLKYKGI	hydrogel	β-sheet (Fig. 1)
SLed *dentinogenic* control peptide	$E(SL)_6E$- G -TDLQERGDNDISPFSGDGQPFKD	hydrogel	β-sheet [13]

catheter to form *in situ* depots that integrate with the host tissue, biodegrade over time, and help regenerate vascularized soft tissues [3,5].

Self-assembling peptides are a class of short (2-50 amino acid) amphiphilic peptides with the canonical sequence Z_a-$(XY)_b$-Z_c, where a, b, and c can be tweaked to optimize material properties, allowing self-assembly into β-sheets (X and Y are hydrophilic and hydrophobic residues, respectively) — with demonstrated utility in numerous *in vitro* and *in vivo* applications [14–16]. These peptides have demonstrated facile injectability as tissue depots, which can be used for wound healing, tissue regeneration, and *in situ* local drug delivery [16,17]. Self-assembly of amphiphilic peptides can be directed to yield ECM-mimic (ECM = extracellular matrix) nanofibrous hydrogels [16–18]. The hydrogels can be injected directly into the target tissue, where they re-gel after injection. The storage moduli of the materials (generally 100–1000 Pa) are especially suitable for facilitating soft-tissue regeneration (e.g., dental pulp, bone marrow, or brain parenchyma) [19].

The therapeutic utility of self-assembling peptides can be extended via modification of the N- or C-terminus with bioactive domains [3,5,17,20]. We have recently reported the development of proangiogenic constructs with the addition of a bioactive mimic from vascular endothelial growth factor (VEGF-165) termed QK to a self-assembling domain [5,14]. These preliminary injectable angiogenic supports established a proof-of-principle for injectable self-assembled growth factor mimics that remain localized for robust neovascularization [3,5,19].

Optimization of biophysical and biochemical properties of angiogenic peptide hydrogels now allow for a versatile range of applications to be explored [13,15,17,18,20,21]. In the previous design of the construct, an MMP-2 cleavage domain in the midblock resulted in rapid degradation [5]. Herein, we have optimized the design of the angiogenic self-assembling peptide sequence (Fig. 1A) by removal of this domain. This angiogenic peptide (termed SLan, Table 1) forms stiff, robust hydrogels, which promotes vascularization in both small and large animal models.

Here, we demonstrate the angiogenic efficacy of SLan in a suitable preclinical translational model — pulp revascularization in adult canine teeth. Pulp revascularization requires defined microvascular regrowth within the tooth root chamber after extirpation of inflamed pulp. The technique is useful for treating juvenile patients after traumatic dental injury and some cases of soft-tissue infection and inflammation. Over-instrumentation of the apex may lead to formation of vascularized pulp-like tissue, if residual apical papilla cells are viable (generally the case in juveniles). If those cells are not present (adults) or not viable (potentially due to apical periodontitis), a muted regenerative response is observed — leading to intracanal avascular ossified tissue formation by periodontal ligament (PDL) or bone marrow cells [22]. Thus, in adults, gutta percha is still widely used as the standard-of-care elastomeric filler for root obturation [23].

Harvested stem cell transplants have shown tremendous clinical potential in recreating intracanal soft tissue niche in large animal models and humans [24]. In contrast, tissue-engineered materials have had more mixed results in recapitulating native microenvironment [25,26]. In spite of showing promise in rodent models, purely materials-based regeneration of sustainable vasculature in the root canal has not been demonstrated in large animal models. We demonstrate that pulp revascularization can be stimulated by implantation of the self-assembling peptide hydrogel SLan in an adult canine teeth after pulpectomy — presenting an acellular materials-based approach to promote pulp-like soft tissue regeneration *in vivo*.

2. Materials and methods

All chemicals were purchased from SigmaAldrich (St. Louis, MO) unless otherwise specified.

2.1. Solid phase peptide synthesis

Peptides were synthesized with a CEM LibertyBlue solid phase peptide synthesizer using standard Fmoc chemistry. The sequences used are shown in Table 1. All peptides were C-terminal amidated and N-terminal acetylated. The crude peptides were cleaved with 2.5% each of H_2O, Triisopropylsilane (TIS), and 3,6-dioxa-1,8-octanedithiol (DoDT) and 92.5% Trifluoroacetic acid (TFA) (10 mL total for 0.1mM scale synthesis) for 30 min at 37°C. The cleaved peptides were crashed out in cold (–20°C) ether, centrifuged, ether decanted, and left to dry overnight. The resulting crude peptide pellets were dissolved in Milli-Q water at a concentration of ~1 mg/mL, pH adjusted to 7, and dialyzed with Spectra/Por S/P 7 RC dialysis tubing at a 2000 Da cutoff tubing against DI water for 3 days. The purified peptides were frozen and lyophilized for at least 3 days, which resulted in a white cotton-like powder. Peptide mass and purity were verified >85% by an Agilent 1100 series HPLC instrument with an Agilent (Santa Clara, CA) C3 reverse phase column. The molecular weights of the peptides were verified with an Orbitrap Q Exactive LC/MS (Thermo Scientific, Waltham, MA) instrument. To verify commercial manufacturing potential, the peptides were manufactured at gram-scale with similar purity (>90%) by AmbioPharm Inc (Beech Island, SC), a manufacturer of peptide APIs for the US market.

2.2. Fourier transform infrared spectroscopy (FTIR)

1% w/v (10 mg/mL) hydrogel samples were prepared for SLan with sucrose and 1X HBSS and were diluted in MilliQ water at 0.1 mg/mL. Samples were pipetted onto the IR plate for spectra analysis between 400 and 4000 cm^{-1} with a background of Milli-Q water subtracted from each reading. The reported spectral region is 1500–1700 cm^{-1} to highlight the amide I and amide II regions.

2.3. Circular dichroism

Circular dichroism (CD) experiments were performed using the Jasco J-810 spectropolarimeter (Oklahoma City, OK, USA). Experiments were conducted at room temperature using a 1 mm cuvette with SLan samples at a concentration of 0.2 mg/mL in HBSS (10 mM HEPES, 150 mM NaCl pH 7.4) buffer at the wavelength range 190–260nm.

2.4. Preparation of nano-porous peptide scaffolds (hydrogel)

SLan was initially dissolved in 298mM sucrose to yield viscous 2% solution. Self-assembling peptides exhibit enhanced self-assembly with the addition of multivalent counterions such as

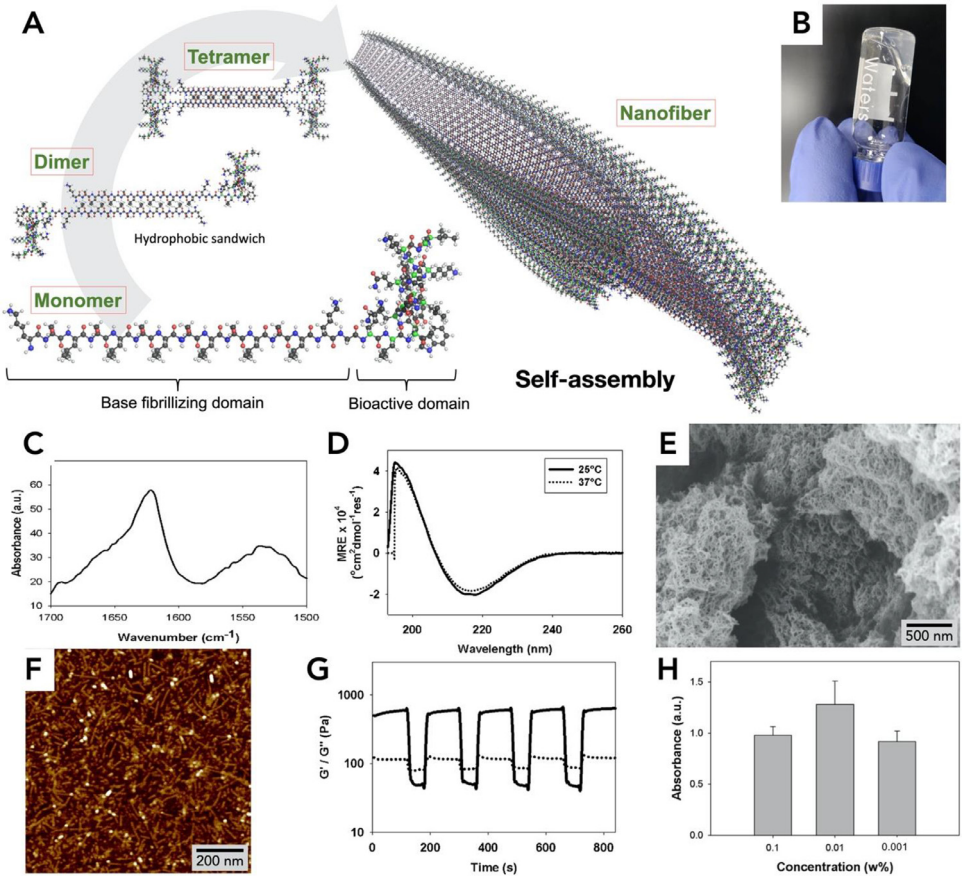

Fig. 1. Biophysical properties of SLan hydrogel. (A) Self-assembly of SLan. In aqueous solution dimers and tetramers form assemble into a β-sheet based nanofibers. (B) 1% SLan hydrogel, (C) FTIR spectrum shows β-sheet secondary structure (1624 cm^{-1} peak) confirmed by (D) Circular dichroism spectra (~195 nm maxima and ~217 nm minima. (E) Scanning electron micrograph of critical-point-dried SLan hydrogel. (F) Individual SLan nanofibers observed in atomic force microscopy. (G) 1% SLan hydrogels are thixotropic. At low strain (1%), G'>G" (indicating solid-like elastic properties), at high strain (100%), G'<G" (signifying liquefaction of the hydrogel and showing dominance of viscous modulus). The switch in rheological properties is fast and reversible (representative plot shown). (H) *In vitro* cytocompatibility (n=4, $p<0.05$, CCK8 dye absorbance) of HEPG2 cells shows that SLan did not exhibit cytotoxicity.

phosphate in PBS or HBSS (to form salt-bridges between the terminal lysines of peptides, Fig. 1). Equivalent volumes of HBSS were added to SLan hydrogels to promote robust hydrogelation.

2.5. Ultrastructural characterization

2.5.1. Scanning electron microscopy

Sample preparation: 200 µL aliquots of 1% SLan hydrogel were crosslinked overnight with 2% glutaraldehyde (Sigma). The crosslinked peptide hydrogels were washed three times with DI water and ethanol dehydrated (50%, 75%, 90%, 95%, 99%, and 100% ethanol/water ratio) for 15 min each. The samples were critical point dried in a Tousimis AutoSambri-795 critical point drying instrument (Rockville, Maryland). The chamber was filled with 100% ethanol ¾ of the way to the top. The samples, submerged in 100% ethanol, were added to the chamber and topped off with 100% ethanol up. The lid on the chamber was secured and evenly tightened. The instrument was switched on and cooled to about 4°C. Liquid ethanol was exchanged for liquid CO_2 under high pressure for 20 min with continuous purging. Samples were maintained in liquid CO_2 for 1 h prior to another 20 min wash with continuous purging. Samples were then heated to 37°C and a pressure of ~1070 p.s.i. At the critical point, the chamber was slowly vented (over 30 min) to prevent condensation of CO_2.

Imaging: The samples were then sputter coated with Au/Pd (8 nm thickness) using an EMS 150 TES sputter coater (Quorum, East Sussex, UK) and imaged with an JSM-7900 (Jeol, Peabody, MA) scanning electron microscope at 5.0 kV accelerating voltage and a working distance of 10 mm.

2.5.2. Atomic force microscopy

Sample preparation: Atomic force microscopy was used to study nanostructure of the peptide. SLan hydrogels were diluted in DI water to 0.1%. Freshly cleaved Mica disks were prepared and adhered by the underside using double-sided tape to a thin metal disk. The diluted peptide solution spin coated by drop-casting 10 µL increments 3x and centrifuging to allow the peptide to evenly spread and dry on the Mica surface.

Imaging: ScanAsyst mode on a Dimension Icon instrument (Bruker, AZ) with sharpened silicon (0.2-0.8 N/m, Al reflective coating) AFM tips (Bruker, AZ) was used to obtain images.

2.6. Rheometry

The viscoelastic properties of the peptide hydrogels were tested with a Kinexus oscillatory rheometer (Malvern Instruments, United Kingdom). Two tests were run: the strain sweep which provides information regarding the injectability of the material, and shear recovery which determines how viscoelastic the material is. In the strain sweep test, 40 µL of hydrogel was pipetted onto the bottom plate of the rheometer and pre-strained for 5 min at constant 1% strain and frequency of 1 Hz with a 4 mm geometry and 250 µm gap (n=4) for 5 min. Immediately after, a strain sweep was run for 5 min with increasing strain (0.1 – 100 % strain). The oscilla-

tory shear recovery test alternates between periods of low strain (1%) and high strain (100%) under the same conditions. This indicates the shear thinning and shear recovery potential and kinetics of hydrogels.

2.7. In vitro cytocompatibility (HEPG2)

Cytocompatibility of SLan peptides was evaluated at 0.1, 0.01, and 0.001% with a mammalian (human) cell (line) that has been extensively used prior: HEPG2 cells (ATCC, Manassas, VA). SLed cytocompatibility *in vitro* has been published [13]. The HEPG2 cells were utilized after their first passage and seeded at a cell density of 10,000 cells/well in a 96 well plate (n=5) in complete HEPG2 media (90% DMEM, 10% FBM, 1% Pen-Strep, and 1% Gluta-max) for 24 hours in an incubator maintained at 37°C and 5% CO_2. The complete HEPG2 media was aspirated and the peptide conditions prepared in serum-free media (DMEM) and control (serum-free media) were introduced. The peptide conditions and controls were incubated for 6 h. The samples were aspirated, the wells were washed with 200 µL of PBS, aspirated once more, 100 µL of PBS was added to each of the wells with 10 µL of CCK8 stain (Dojindo, Japan). After 1 h incubation, the 96 well plate was read in a TECAN M200 Infinite plate reader at an absorbance of 450 nm against a reference wavelength of 650 nm. The results were analyzed and normalized to the serum-free media control.

2.8. Subcutaneous (sub-Q) implantation

All animals were treated in accordance with NJIT-Rutgers Newark Institutional Animal Care and Use Committee (IACUC) and AALAC guidelines. Female Wistar rats (250-275 g) were used for dorsal subcutaneous implantation. The rats were anesthetized using 2.5% isoflurane for induction and 1.5% for maintenance, followed by shaving of dorsal regions, isopropanol, and betadine sterile-preparation of the surgical site. For sub-Q hydrogel implants, 200 µL boluses of SLan 1% hydrogels were injected in n=4 per timepoint – 7, 14, and 28 days. At 7 (acute), 14, and 28 days rats were sacrificed, and implant regions were excised. Harvested tissue sections were immediately fixed with 10% formalin. Samples were then processed by the histology core at the Rutgers Cancer Institute of New Jersey. The formalin embedded sections were ethanol series dehydrated, solvent exchanged for xylene, and then paraffin using a tissue processor. Samples were blocked in paraffin, sectioned to 6–8 µm sections, and stained using hematoxylin and eosin (H&E) or Masson's Trichrome (MT) (SigmaAldrich, St. Louis, MO). Other sections were deparaffinized and immuno-stained (protocol and reagents detailed below).

2.9. Pulp revascularization model

All studies were approved by the Rutgers-NJIT IACUC committee and followed USDA guidelines. Adult male Beagles' incisors were used to evaluate pulp revascularization after a full pulpectomy. In two Adult Beagles' (22–26 months of age, male), 6 maxillary and 6 mandibular incisors were cleaned and exposed (n=12 implant sites for each canine). Using this model, we were able to see clear differences in the tissue regenerative response in each tooth, independent of adjacent teeth – minimizing the number of canines used. Animals were sedated with ketamine and diazepam, anesthetized with isoflurane and intubated. They were dosed perioperatively and post-operatively with buprenorphine for pain management and convenia for potential infections.

The oral cavity (including teeth) was cleaned by Peridex (0.12% Chlorhexidine rinse). A round diamond bur attached to a high-speed handpiece was used to drill through to the pulp chamber. The pulp tissues were removed by H-files (#10). At same time, the working length was measured by an Apex locator. The canal spaces were expanded by K-files (#10-30). The canal space and apical area were widened by the Rotary Niti files (S1-F3) with Endo motor handpiece. The canal space was irrigated by 5.25% sodium hypochlorite and then PBS. As is standard procedure, to induce growth factors from the dentin matrix, 17% EDTA was soaked in the canal space for 5 min. The canal space was then irrigated with phosphate buffered saline (PBS). To manage apical breeding, paper points were utilized. Uniform root canals were filled with 10–25 µL of hydrogels (SLan, SLed, SLan+SLed (50:50)), PBS). Composite resins were sealed at the top of canal spaces. At 28 days, animals were sedated and anesthetized as above, the 12 teeth were extracted, washed in PBS and immediately placed in formalin for 24 hours followed by decalcification using 10% EDTA for 21 days. Samples were processed by the histology core at the Rutgers Cancer Institute of New Jersey. The decalcified teeth samples were blocked in paraffin, sectioned to 5-8 µm sections and stained using H&E, MT, or immuno-stained, as above.

2.10. Immunostaining

Sections were de-paraffinized in 5% xylene for 10 min, then 100%, 95%, 90%, 70%, 60%, 50% ethanol, and water and then immersed in PBS three times at 3 min each. The de-paraffinized samples were washed with PBS for 5 min. Then 2% bovine serum albumin was used to block non-specific absorption for 30 min. Samples were then immuno-stained with 3 different antibodies and counterstained with DAPI: i) Dental sialoprotein (DSP, Santa Cruz Sc33587) at 1/400 dilution in antibody buffer, 4°C overnight; secondary: Dk-anti-rb-FITC (Invitrogen 488 Alexa Fluor A21206), at 1/1000 dilution for 30 min. ii) S-100 (ab14849, Ms-anti-rb) at 1/400 dilution in antibody buffer, 4°C overnight; secondary: Dk-anti-ms-NL557 at 1/200 dilution for 30 min. iii) PECAM (bs-0468R, Rb anti-Rt) at 1/400 dilution in antibody buffer, 4°C overnight; secondary: Dk-anti-rb-FITC (Invitrogen 488 Alexa Fluor A21206), at 1/1000 dilution for 30 min. Then the samples were washed with PBS again 3 times for 5 min each. Mounting media with DAPI (Invitrogen SlowFade Diamond Antifade Mountant with DAPI) was used as a mountant in coverslipping. A Leica SP8 microscope (Leica, Switzerland) was used to image samples using conventional confocal and fluorescent microscopy techniques.

2.11. Implant image analysis (QuPath)

The cell density, infiltration, collagen deposition, blood vessel density and degree of regeneration for subcutaneous and pulp revascularization samples were calculated using the program QuPath [27]. The polygon tool was used to draw along the border of the entire implant. The cell detection tool was selected to adjust threshold and minimum area parameters to get the most accurate count of cells (threshold usually set between 10 and 15 and area set between 5 and 10). Cell detection was executed with the area of region and number of cells recorded. The area was converted from pixels to mm based on image scale bar size conversion factors. The cell density was determined by dividing the number of cells by outlined area in mm^2. The blood vessel density was calculated within each region and determined by dividing the number of blood vessels by outlined area in mm^2. Analyses were performed across all the regions within each slide (n=4 regions per slide), and then all slides (n=4 different implants per group) for 7-day, 14-day, and 28-day samples.

2.12. Data analysis and statistical evaluation

Data is represented as Mean ± standard deviation. Differences between paired data were compared using Student's t-test. ANOVA

with Tukey post hoc analysis was used for multiple comparisons of parametric data, and Kruskal Wallis ANOVA with Dunn's post hoc analysis was used for non-parametric data. Values of $p < 0.05$ were considered statistically significant.

3. Results

3.1. Facile synthesis of an angiogenic cytocompatible hydrogel

SLan (an acronym derived from the midblock (Serine-Leucine) repeats with an appended angiogenic domain) has a central self-assembling domain with a high β-sheet propensity (Fig. 1A). The peptide is easily synthesized and purified by standard solid-phase peptide synthesis to yield a lyophilized powder. Lyophilized SLan self-assembles into nanofibers in aqueous solution as shown in Fig. 1A, forming a hydrogel (Fig. 1B). These peptides self-assemble through β-sheet formation, as shown via the FTIR peak at 1624 cm^{-1} (Fig. 1C) and circular dichroism (CD) minima at 217 nm, at both room temperature (25°C) and at physiological temperature (37°C) (Fig. 1D). The cross-linked nanofibrous mesh constituting the hydrogel was imaged by scanning electron microscopy (SEM) (Fig. 1E), and the individual self-assembled nanofibers were observed by atomic force microscopy (AFM) (Fig. 1F).

The underlying nanofibrous architecture corresponds to a thixotropic hydrogel at the bulk scale. The hydrogel is reversibly shear-responsive (Fig. 1G) [18]; thus can be easily injected *in vivo*, where it is re-constituted into a stiff bolus. SLan has similar biophysical properties to other self-assembling peptides within this platform (Table 1) [13,14,18,20,21]. SLan has a proangiogenic "QK" domain derived from VEGF-165, presented at a constitutively high epitope density within self-assembled nanofibers (Fig. 1A) [28]. Optimization of SLan over previous angiogenic SAP [5] by removal of an MMP-2 susceptible –LRG– midblock sequence promotes robust hydrogelation and prolongs *in vivo* persistence. *In vitro* cytocompatibility utilizing the CCK8 metabolic dye showed compatibility with mammalian HEPG2 cells (Fig. 1H); SLan did not exhibit any cytotoxicity normalized to serum-free media control.

3.2. Biocompatibility

Biocompatibility of SLan was confirmed *in vivo* our benchmarked subcutaneous biocompatibility model [5]; 200 µL boluses were injected subcutaneously (sub-Q) under the backs of adult rats. Peptide hydrogels degraded over a 1-month period (Fig. 2A–F). Cells rapidly infiltrated scaffolds (without any fibrous encapsulation) and promoted the development of vasculature and deposition of collagen within implants (Fig. 2G–L). Cell density within implants decreased over time owing to the degradation of the hydrogel (Fig. 2M). The number of blood vessels increased from 7-14 days but resorbed by 28 days (Fig. 2N). The degree of infiltration consequently showed a marked decrease after scaffolds had degraded (Fig. 2O). These results show that the bolus angiogenic peptide hydrogels stay localized after injection and degrade leaving native tissue over a 28 day period. Notably, no animals tested with these scaffolds (of the hundreds of rodents tested within the SAP platform) have shown incidence of systemic side effect, tumorigenicity or adverse side effect (up to 10 mg SC in a 200-250 g rat) [5,13,15,17]. The use of the rat sub-Q model allows for determination of preliminary safety to large doses (~10 mg/kg) compared to intratooth canine implants below (~0.05 mg/kg).

3.3. Material-guided dental pulp revascularization

After full pulpectomies, the pulp canals of the canines were irrigated. Bleeding was managed using paper points before filling the extirpated canals with 15–50 µL of SLan, carrier, control peptide SLed, or 1:1 SLan+SLed (Fig. 3, S1). Terminal explants at 28 days showed poor disorganized tissue in growth in carrier and non-SLan SAP (SLed, Table 1) filled teeth (Fig. 3D,G). SLan-filled teeth showed organized soft tissue in the canal (Fig. 3E,F,H,I), with collagen deposition and large, clearly visible vessels carrying red blood cells (Fig. 3H–I). Nerve bundles are visible (Fig. 3I (#), L) with an odontoblast-like layer apposed to the intracanal dentin (Fig. 3I–K, S2), representing tissue regeneration within implants (Fig. 3N). Importantly, in all 8 SLan treated teeth, at Day 28, implants were free of any observable calcification or disorganized hard tissue, and all had significant cellular infiltration, matrix deposition, and DSP^{+} cells (with signs of protrusions into dentinal tubules, Fig. 3J,K). These findings, along with robust revascularization (Fig. 3O) fulfill key features of biomaterials needed for targeted *in situ* regeneration of the dental pulp [13,29] (Table S1). Overall, we show that SLan is capable of consistently regenerating vascularized tissue in the canine pulp space. Prior to the canine studies, we screened and eliminated a number of self-assembling peptides in rodent sub-Q studies, as they did not fulfill our target criteria. We have previously shown that a pro-dentinogenic SAP (SLed, Table 1) promotes *in vitro* dental pulp stem cell proliferation [13], but in our canine *in vivo* experiments, SLed failed to revascularize pulp, compared to the angiogenic peptide SLan, despite having similar material properties (Fig. 3M–O).

4. Discussions

4.1. Optimal biophysical properties

Self-assembly of SLan into a thixotropic hydrogel (Fig. 1A–B) yields a cytocompatible material that not only has an ECM-mimetic ultrastructure (Fig. 1E–F), but also contains a VEGF-mimicking bioactive domain in its primary sequence. Our work builds on a growing literature of acellular supramolecular biomaterials [30,31], especially those with bioactive domains encoded directly in the scaffold [5,14,20,32]. The β-sheet conformation of the supramolecular nanofiber leads to presentation of this active moiety at a high density to cell-surface receptors [3]. Such functionalizability is the principal advantage of the therapeutic platform. However, the functionalization strategy rests on the high propensity of the core amphiphilic domain to form nanofibers in physiological pH and ionic strength [16–18,33]. The nanofibrous architecture is key to mimicking native extracellular matrix at a subcellular scale, and the resultant hydrogels have viscoelastic properties similar to soft tissues.

4.2. Establishment of angiogenic niche in vivo

SLan presents a versatile platform to develop tailorable vascularized tissues *in vivo* that may have broad impact in vascularizing ischemic tissue, wound healing, and replacing injured soft tissue. Alone, SLan results in robust angiogenesis and rapid vascularization of mature blood vessels within 7 days. In the subcutaneous niche, SLan induced formation of new vasculature and matrix deposition in 28 days. When supporting tissue ingrowth in tissue voids (tooth root canal), SLan promotes robust and sustained vascularization and soft tissue regeneration via scaffold-based signaling (Fig. 2). It's interesting to note that the degradation of SLan hydrogels seem to be faster in the subcutaneous niche (Fig. 2), compared to the intra-dental microenvironment (Fig. 3). We ascribe the difference to the variance of access to peripheral circulation (and hence clearance by immune cells such as macrophages).

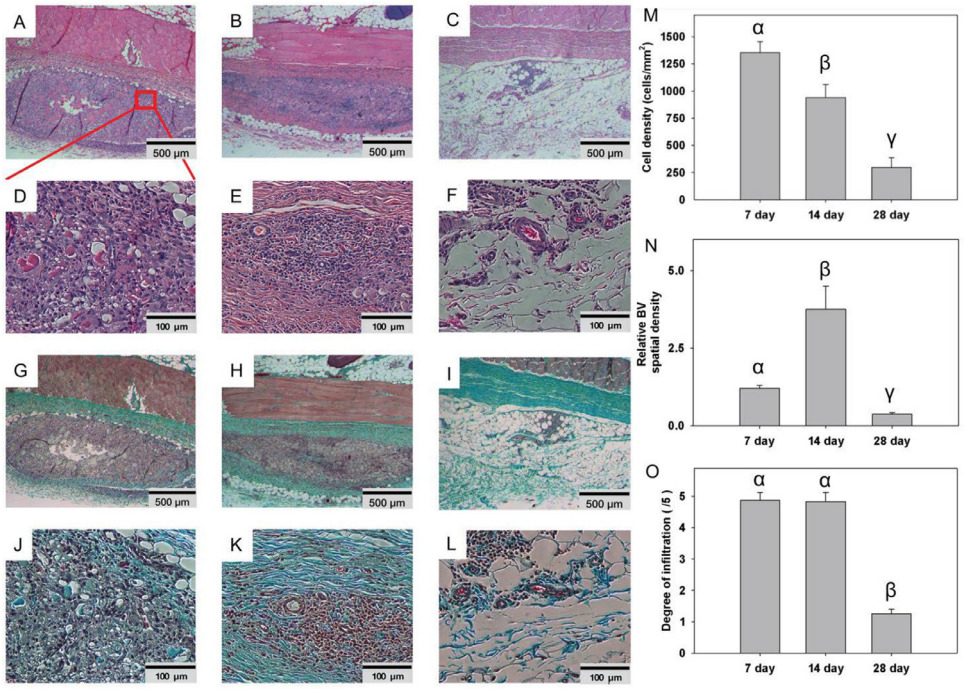

Fig. 2. Dorsal subcutaneous implants of SLan in rats. Implants (n=4) showed rapid infiltration of cells - H&E images of 200 µL bolus implants in Wistar rats as early as Day-7 (A: 500 µm, region magnified in D: 100 µm), completely into the center of implants by Day 14 (B: 500 µm, E: 100 µm), and fully degraded by Day 28 (C: 500 µm, F: 100 µm). Similarly, extracellular matrix (ECM) deposition (collagen, blue) was noted in Masson's Trichrome staining, with infiltration of blood vessels as early as 7 days (G: 500 µm, J: 100 µm), Day 14 (H: 500 µm, K: 100 µm), with complete resorption of superfluous collagen and vasculature by 28 days (I: 500 µm, L: 100 µm). (M) Cell density analysis of 7,14, and 28 day SLan rat subcutaneous samples. (N) Blood vessel density analysis of 7,14, and 28 day SLan rat subcutaneous samples. (O) Degree of infiltration analysis of 7, 14, and 28 day SLan rat subcutaneous samples.

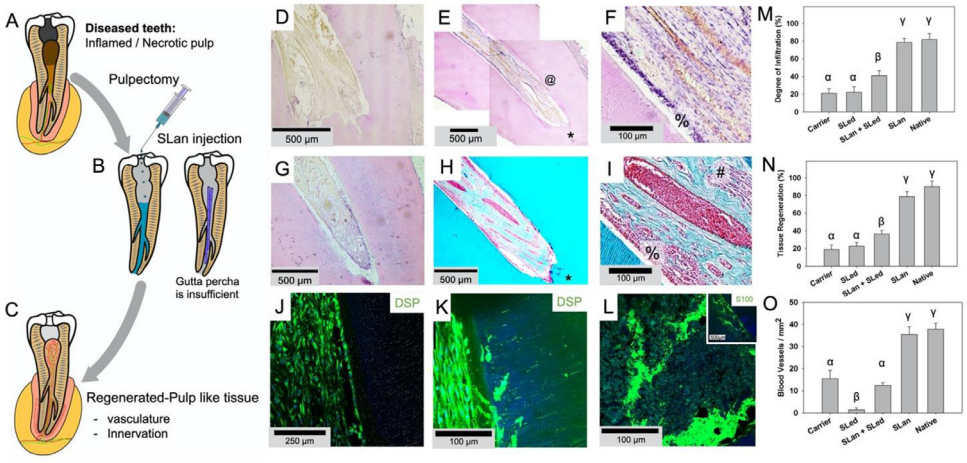

Fig. 3. Regeneration of vascularized soft tissue in canine root canals. (A) Caries and trauma may lead to the inflammation and necrosis of the pulp (A). (B) After pulpectomy, implantation of injectable angiogenic SLan hydrogels help regenerate (C) vascularized pulp-like soft tissue in 28 days, unlike inert materials such as gutta percha. In a canine pulpectomy model, disorganized blood clots form for over-instrumentation carrier filled (sucrose-HBSS) control (D). H&E staining of tooth roots of SLan filled teeth showed rapid infiltration of cells and tissue (E), and within crevices in the canal space (@), along with an odontoblast-like layer in apposition to the dentin wall (F - %). In contrast, control dentinogenic SLed hydrogels lead to disorganized tissue (G). Trichrome staining of SLan implants reveals blood vessels (H, I) with collagen deposition (blue); and an odontoblast-like layer (I - %) which stains with dental sialoprotein (DSP) (J) with cytoplasmic protrusions into dentinal tubules (K). S100⁺ Nerve bundles (Trichrome I-#) were regenerated along the length of the canal (L and inset). (M) Degree of infiltration, (N) degree of tissue regeneration, and (O) densities of blood vessels were similar for SLan and native teeth but significantly greater than controls. (n=8 for SLan, n=4 for all other groups; values are reported as mean ± standard deviation; different Greek letters indicate statistical significance between groups $p<0.05$).

4.3. Challenges for dental pulp tissue engineering & pulp-revascularization therapy

Teeth are complex organs as a target for tissue regeneration. It hosts one of the softest tissues in our body (pulp) right next to the hardest tissues (enamel and dentin). It has been recognized as early as 1931 that dentinal injury adversely affects the dental pulp and the pulp-dentin complex [34], and recent investigations demonstrate the active role of dental pulp cells in repairing dentin after traumatic injury [35]. Both enamel and dentin are avascular and the apical foramen is the sole source of blood supply to the pulpal soft tissue [36]. If the dental pulp is replaced, the nutrient supply to the remodeled tissue may be disrupted, unless the tissue facilitates angiogenic sprouting into the niche. The peripheral

circulation is also a potential source for infiltrating immune and progenitor cells into the pulpal cavity.

Pulp revascularization therapy is currently accepted by the American Dental Association and the American Association of Endodontics as a treatment modality to revitalize the tooth after pulp damage [37]. Over-instrumentation can be used over root obturation (blocking/filling with gutta percha), especially in young patients, as the inert elastomeric material is an impediment to tissue remodeling in patients with open root apices [38]. Over-instrumented teeth result in blood clots (fibrin scaffolds) that resorb (~7 days) and allow tissue infiltration. Periapical tissues including survived apical papilla cells and periodontal ligament cells can proliferate in the pulp space afterwards. Infiltrating tissue leads to markedly differential responses depending on the age of the animals and procedural technique used. In adult humans, over-instrumentation has poor success rates, due to the absence of apical papilla cells and a lack of suitable matrix to support infiltrating cells and essential vasculature [23]. An off-the-shelf material-based strategy that consistently regenerates vascularized pulp like tissue is critically needed.

4.4. Features of the regenerated soft tissue

We demonstrate that acellular SLan hydrogel scaffolds consistently regenerate vascularized organized soft tissue in the canal space post-pulpectomy in adult canines (Fig. 3). As we combined over-instrumentation with material implantation, we were able to use an acellular formulation, as the matrix then has access to infiltrating cells. In SLan hydrogel implants, a column of DSP^+ odontoblast-like cells (DSP = dental sialoprotein) formed apposed to the dentinal tubules (Fig. 3F,I,J, also see Fig. S3 and Fig. S4 in the Supplementary Information). Such an odontoblast layer is present in native tissue and similar layers have been recapitulated by stem cell delivery in minipig models [24,39]. The DSP^+ cells formed at the periphery of the SLan implant send cellular protrusions into dentinal tubules (Fig. 3K), similar to odontoblast processes observed in native tissue [40]. The identity, source, and lineage of the DSP^+ cells need further investigation, to distinguish them from osteo-odontogenic cells. Longer term studies may help define stability of the regenerated soft tissue and possible induction of osteogenesis/mineralization by infiltrating cells.

An unexpected but encouraging observation in our studies was that the regenerated soft tissue in the canal not only contained blood vessels, but also $S100^+$ peripheral nerve fascicles (Fig. 3I,L) [41]. In retrospect, this data conforms to previous reports of co-formation of nerve filaments and blood vessels in implanted self-assembling hydrogel scaffolds [17]. In addition, angiogenic factors also tend to be nerve-guiding factors, and axonal growth cones share structural similarities with endothelial tip cells crucial for angiogenesis [42]. Nerves in the dental pulp detect pain sensation [43] and the perineural niche has been identified as a source of stem cells [44,45] — thus innervation of the scaffold has functional implications. Based on prior studies, the odontoblast-like layer, blood vessels, and the nerve filaments may be potentially derived from stem cells recruited from the apical papilla, the periodontal ligament, or the bone marrow (via peripheral circulation) [23,46–48].

4.5. Choice of the animal model

Ectopic subcutaneous implantation of tooth slices in immunocompromised mice remains an important model for testing materials and stem cells for pulp and dentin regeneration [25,49–54], and for exploring mechanistic pathways to facilitate cellular reprogramming into regenerative phenotypes [48,55]. However, for translational purposes they are inferior to orthotopic models [24,48], such as the one employed in this study — since the latter exposes the pulpal chamber to naturally occurring signals present in its native environment. The immunocompromised mouse models often lack adaptive immune responses and thus cannot recapitulate a critical complexity of human pathology.

We selected a *non-immunocompromised* orthotopic canine model as our preclinical model since: (a) the anatomy and size of canine teeth closely mimic human teeth [56], (b) the healing process is similar, and (c) adult canines have tapered growth curves and maturation into adulthood like humans (vs. teeth of rodents that continue to grow till death) [13,29,57–59]. Our selection is congruent with the use of the canine models for preclinical studies [29,59–65], although we acknowledge the limitation that dogs have dental radicular anatomy distinct from humans (e.g., spider-webbed foramina instead of a single foramen), and alternative minipig models have been successfully used for other pre-clinical studies [24,48]. Our animal model of choice is also superior to orthotopic rodent models [66,67], as rodent teeth have permanent open apices and show dental pulp regeneration after over-instrumentation in mature animals, unlike adult dogs (and humans).

4.6. Comparison with previous tissue-engineering strategies

Stem cell delivery, with or without added growth factors and scaffolds, have been the major thrust of dental pulp tissue engineering [24–26,39,49,50,52–54,61–65,68]. Choice of stem cells, especially after full pulpectomy, is appealing as they can differentiate into both the parenchyma and the stroma of the dental pulp. Stem cell therapy has been tested for dental pulp regeneration in large animals [24,39,61–65,68] and in a preclinical human trial [24]. As our approach does not involve added stem cells, we attribute the success of our strategy to migration of endogenous cells into the implanted scaffold, thus the combination of material implantation with over-instrumentation can yield some of the same regenerative benefits as stem cell transplantation.

Implanted scaffolds may help support soft tissue remodeling. Some of the materials that have been used for pulp regeneration include peptide hydrogels [25,26,49], collagen [48,49], silk fibroin [65], and various polymeric scaffolds [39,51,67,69]. The functional self-assembling peptide hydrogel that we characterized builds on these advances by encoding bioactive signals directly in the sequence. Although VEGF-loaded scaffolds have shown limited promise in ectopic tooth slice models [25,51,69], we improve on these results by demonstrating success of scaffolds with VEGF-mimicking functionality in a large animal model. Similar VEGF-mimic scaffolds have demonstrated ability to facilitate formation of smooth muscle lined mature blood vessels in implants [5,14].

Mao and colleagues have reported that recombinant Wnt3a delivered in a decellularized collagen gel can help regenerate vascularized pulp-like tissue post-pulpectomy (by recruiting endogenous cells) in an orthotopic pig model [48]. The study unequivocally demonstrates that it's possible to regenerate pulpal vasculature after complete removal of the pulp *without cell transplantation, in a large animal model*. Similar to our work, this acellular formulation enabled formation of $S100^+$ nerve filaments in the regenerated soft tissue [48].

Stem cells, recombinant factors, and decellularized matrices have batch-to-batch variabilities, sourcing issues, and problems with scaling up, all of which can be avoided by synthetic biomimetic matrices such as SLan. Scaffold-based signaling, as employed by SLan, obviates two elements of the cell-signal-scaffold triad [70] in cases where the scaffold has access to infiltrating endogenous cells [71], and thus has an operational elegance that may be useful for clinical applications and the economy of scale.

4.7. Limitations & future direction

While SLan addresses key features of pulp regenerative materials (Table S1), further experiments are needed to evaluate radiographic root thickening, root lengthening, and pulp sensitivity. Bridging a critical barrier in the field, SLan-based angiogenesis presents a crucial step in developing intracanal materials, providing an option for patients who do not have the time to wait for the expansion of autologous stem cells, and who may have immune sensitivity to recombinantly expressed biologics, or who can't afford costly transplant treatments. The low cost of material synthesis indicates the potential for widespread translatability in clinical care [13,29,57,59].

Critically, we demonstrate the versatility of injectable off-the-shelf SLan for vascularized tissue regeneration and material only efficacy in pulp revascularization in a large animal (adult canine) model. Overall, SLan may present a robust vascularizing hydrogel with demonstrated utility and efficacy in a variety of tissue regeneration strategies. The clinical potential of the acellular biomaterial approach may be extended to include antimicrobial activity [18] and neuroprotective functionality [20] in the scaffold and encapsulating complementary soluble factors [72].

5. Conclusions

We demonstrate that a soft biomimetic acellular peptide hydrogel can recapitulate the vascular niche in the dental root canal after pulpectomy. Presentation of a growth-factor mimic within the primary sequence of the constituent peptide enables retention of angiogenic functionality *in vivo* for up to a month. The material property of the hydrogel is similar to native dental pulp and in a canine pulpectomy model the material facilitates excellent biointegration and soft tissue regeneration. Supramolecular peptide hydrogels promise to be a great addition to our tools for tissue engineering [3,16,31,73,74], as functional acellular biomaterials [30].

Data availability

All analyzed data are presented in the published article. Readers can request raw data for reproducing results from the corresponding author (V.A.K.).

Funding

We would like to thank NJIT startup funds (for V.A.K.) as well as NJIT Undergraduate Research and Innovation (URI) program. V.A.K. acknowledges support from the National Eye Institute NIH R15 EY029504 and National Science Foundation NSF IIP 1903617, NIH R01DE025885 (for E.S), NIH R01 AR072731 (for J.Y.).

Supplementary Information

Supplementary materials associated with this article can be found in the online version.

Declaration of Competing Interest

The authors declare that they have no known competing financial interests or personal relationships that could have appeared to influence the work reported in this paper.

.A.K. has equity interests in commercialization ventures to translate these and related technologies.

CRediT authorship contribution statement

Zain Siddiqui: Investigation, Methodology, Visualization, Formal analysis, Writing – original draft, Writing – review & editing. **Biplab Sarkar:** Conceptualization, Methodology, Visualization, Formal analysis, Writing – original draft, Writing – review & editing. **Ka-Kyung Kim:** Investigation, Methodology, Writing – review & editing. **Nurten Kadincesme:** Investigation, Methodology, Writing – review & editing. **Reshma Paul:** Investigation, Methodology, Writing – review & editing. **Arjun Kumar:** Investigation, Methodology, Writing – review & editing. **Yoshifumi Kobayashi:** Investigation, Methodology, Writing – review & editing. **Abhishek Roy:** Investigation, Methodology, Writing – review & editing. **Marwa Choudhury:** Investigation, Methodology, Writing – review & editing. **Jian Yang:** Supervision, Project administration, Resources, Writing – review & editing, Funding acquisition. **Emi Shimizu:** Conceptualization, Methodology, Writing – review & editing, Funding acquisition. **Vivek A. Kumar:** Conceptualization, Methodology, Supervision, Project administration, Resources, Writing – original draft, Writing – review & editing, Funding acquisition.

Acknowledgments

General: We would like to thank the Materials Characterization Core at NJIT for materials characterization. We thank Dr. William Windsor and Candice Casillas for conducting and analyzing circular dichroism spectra. We would like to thank Kamiya Patel, Sreya Sanyal, Disha Panchal, Paolo Elguera, Shareef Syed, Maria Pepper and Aryan Mahajan for critical analysis, feedback, edits and illustration efforts.

Supplementary materials

Supplementary material associated with this article can be found, in the online version, at doi:10.1016/j.actbio.2021.03.001.

References

[1] H.G. Augustin, G.Y. Koh, Organotypic vasculature: from descriptive heterogeneity to functional pathophysiology, Science 357 (6353) (2017) eaal2379, doi:10.1126/science.aal2379.
[2] P. Carmeliet, R.K. Jain, Molecular mechanisms and clinical applications of angiogenesis, Nature 473 (7347) (2011) 298–307.
[3] B. Sarkar, P.K. Nguyen, W. Gao, A. Dondapati, Z. Siddiqui, V.A. Kumar, Angiogenic self-assembling peptide scaffolds for functional tissue regeneration, Biomacromolecules 19 (9) (2018) 3597–3611.
[4] V. Mastrullo, W. Cathery, E. Velliou, P. Madeddu, P. Campagnolo, Angiogenesis in tissue engineering: as nature intended? Front. Bioeng. Biotechnol. 8 (2020) 188.
[5] V.A. Kumar, Q. Liu, N.C. Wickremasinghe, S. Shi, T.T. Cornwright, Y. Deng, A. Azares, A.N. Moore, A.M. Acevedo-Jake, N.R. Agudo, S. Pan, D.G. Woodside, P. Vanderslice, J.T. Willerson, R.A. Dixon, J.D. Hartgerink, Treatment of hind limb ischemia using angiogenic peptide nanofibers, Biomaterials 98 (2016) 113–119.
[6] R. Khurana, M. Simons, J.F. Martin, I.C. Zachary, Role of angiogenesis in cardiovascular disease: a critical appraisal, Circulation 112 (12) (2005) 1813–1824.
[7] B.H. Annex, Therapeutic angiogenesis for critical limb ischaemia, Nat. Rev. Cardiol. 10 (7) (2013) 387–396.
[8] J.D. Weaver, D.M. Headen, J. Aquart, C.T. Johnson, L.D. Shea, H. Shirwan, A.J. Garcia, Vasculogenic hydrogel enhances islet survival, engraftment, and function in leading extrahepatic sites, Sci. Adv. 3 (6) (2017) e1700184.
[9] A.R. Amini, C.T. Laurencin, S.P. Nukavarapu, Bone tissue engineering: recent advances and challenges, Crit. Rev. Biomed. Eng. 40 (5) (2012) 363–408.
[10] P.S. Briquez, L.E. Clegg, M.M. Martino, F.M. Gabhann, J.A. Hubbell, Design principles for therapeutic angiogenic materials, Nat. Rev. Mater. 1 (1) (2016) 15006.
[11] B. Grigoryan, S.J. Paulsen, D.C. Corbett, D.W. Sazer, C.L. Fortin, A.J. Zaita, P.T. Greenfield, N.J. Calafat, J.P. Gounley, A.H. Ta, F. Johansson, A. Randles, J.E. Rosenkrantz, J.D. Louis-Rosenberg, P.A. Galie, K.R. Stevens, J.S. Miller, Multivascular networks and functional intravascular topologies within biocompatible hydrogels, Science 364 (6439) (2019) 458–464.
[12] R. Gianni-Barrera, N. Di Maggio, L. Melly, M.G. Burger, E. Mujagic, L. Gurke, D.J. Schaefer, A. Banfi, Therapeutic vascularization in regenerative medicine, Stem Cells Transl. Med. 9 (4) (2020) 433–444.
[13] P.K. Nguyen, W. Gao, S.D. Patel, Z. Siddiqui, S. Weiner, E. Shimizu, B. Sarkar, V.A. Kumar, Self-assembly of a dentinogenic peptide hydrogel, ACS Omega 3 (6) (2018) 5980–5987.

[14] V.A. Kumar, N.L. Taylor, S. Shi, B.K. Wang, A.A. Jalan, M.K. Kang, N.C. Wickremasinghe, J.D. Hartgerink, Highly angiogenic peptide nanofibers, ACS Nano 9 (1) (2015) 860–868.
[15] T.L. Lopez-Silva, D.G. Leach, A. Azares, I.C. Li, D.G. Woodside, J.D. Hartgerink, Chemical functionality of multidomain peptide hydrogels governs early host immune response, Biomaterials 231 (2020) 119667.
[16] A.N. Moore, J.D. Hartgerink, Self-assembling multidomain peptide nanofibers for delivery of bioactive molecules and tissue regeneration, Acc. Chem. Res. 50 (4) (2017) 714–722.
[17] A.N. Moore, T.L. Lopez Silva, N.C. Carrejo, C.A. Origel Marmolejo, I.C. Li, J.D. Hartgerink, Nanofibrous peptide hydrogel elicits angiogenesis and neurogenesis without drugs, proteins, or cells, Biomaterials 161 (2018) 154–163.
[18] B. Sarkar, Z. Siddiqui, P.K. Nguyen, N. Dube, W. Fu, S. Park, S. Jaisinghani, R. Paul, S.D. Kozuch, D. Deng, P. Iglesias-Montoro, M. Li, D. Sabatino, D.S. Perlin, W. Zhang, J. Mondal, V.A. Kumar, Membrane-disrupting nanofibrous peptide hydrogels, ACS Biomat. Sci. Eng. 5 (9) (2019) 4657–4670.
[19] X. Ma, A. Agas, Z. Siddiqui, K. Kim, P. Iglesias-Montoro, J. Kalluru, V. Kumar, J. Haorah, Angiogenic peptide hydrogels for treatment of traumatic brain injury, Bioact. Mater. 5 (1) (2020) 124–132.
[20] B. Sarkar, X. Ma, A. Agas, Z. Siddiqui, P. Iglesias-Montoro, P.K. Nguyen, K.K. Kim, J. Haorah, V.A. Kumar, In vivo neuroprotective effect of a self-assembled peptide hydrogel, Chem. Eng. J. 408 (2021) 127295, doi:10.1016/j.cej.2020.127295.
[21] P.K. Nguyen, B. Sarkar, Z. Siddiqui, M. McGowan, P. Iglesias-Montoro, S. Rachapudi, S. Kim, W. Gao, E. Lee, V.A. Kumar, Self-assembly of an anti-angiogenic nanofibrous peptide hydrogel, ACS Appl. Bio Mater. 1 (3) (2018) 865–870.
[22] E. Shimizu, D. Ricucci, J. Albert, A.S. Alobaid, J.L. Gibbs, G.T. Huang, L.M. Lin, Clinical, radiographic, and histological observation of a human immature permanent tooth with chronic apical abscess after revitalization treatment, J. Endod. 39 (8) (2013) 1078–1083.
[23] E. Shimizu, G. Jong, N. Partridge, P.A. Rosenberg, L.M. Lin, Histologic observation of a human immature permanent tooth with irreversible pulpitis after revascularization/regeneration procedure, J. Endod. 38 (9) (2012) 1293–1297.
[24] K. Xuan, B. Li, H. Guo, W. Sun, X. Kou, X. He, Y. Zhang, J. Sun, A. Liu, L. Liao, S. Liu, W. Liu, C. Hu, S. Shi, Y. Jin, Deciduous autologous tooth stem cells regenerate dental pulp after implantation into injured teeth, Sci. Transl. Med. 10 (455) (2018) eaaf3227, doi:10.1126/scitranslmed.aaf3227.
[25] K.M. Galler, J.D. Hartgerink, A.C. Cavender, G. Schmalz, R.N. D'Souza, A customized self-assembling peptide hydrogel for dental pulp tissue engineering, Tissue Eng. Part A 18 (1–2) (2012) 176–184.
[26] F. Mangione, M. EzEldeen, C. Bardet, J. Lesieur, M. Bonneau, F. Decup, B. Salmon, R. Jacobs, C. Chaussain, S. Opsahl-Vital, Implanted dental pulp cells fail to induce regeneration in partial pulpotomies, J. Dent. Res. 96 (12) (2017) 1406–1413.
[27] P. Bankhead, M.B. Loughrey, J.A. Fernandez, Y. Dombrowski, D.G. McArt, P.D. Dunne, S. McQuaid, R.T. Gray, L.J. Murray, H.G. Coleman, J.A. James, M. Salto-Tellez, P.W. Hamilton, QuPath: Open source software for digital pathology image analysis, Sci. Rep. 7 (1) (2017) 16878.
[28] L.D. D'Andrea, G. Iaccarino, R. Fattorusso, D. Sorriento, C. Carannante, D. Capasso, B. Trimarco, C. Pedone, Targeting angiogenesis: structural characterization and biological properties of a de novo engineered VEGF mimicking peptide, Proc. Natl. Acad. Sci. U. S. A. 102 (40) (2005) 14215–14220.
[29] M. Nakashima, K. Iohara, M.C. Bottino, A.F. Fouad, J.E. Nor, G.T. Huang, Animal models for stem cell-based pulp regeneration: foundation for human clinical applications, Tissue Eng. Part B Rev. 25 (2) (2019) 100–113.
[30] J.A. Burdick, R.L. Mauck, J.H. Gorman 3rd, R.C. Gorman, Acellular biomaterials: an evolving alternative to cell-based therapies, Sci. Transl. Med. 5 (176) (2013) 176ps4.
[31] M.J. Webber, E.A. Appel, E.W. Meijer, R. Langer, Supramolecular biomaterials, Nat. Mater. 15 (1) (2016) 13–26.
[32] M.J. Webber, J. Tongers, C.J. Newcomb, K.T. Marquardt, J. Bauersachs, D.W. Losordo, S.I. Stupp, Supramolecular nanostructures that mimic VEGF as a strategy for ischemic tissue repair, Proc. Natl. Acad. Sci. U. S. A. 108 (33) (2011) 13438–13443.
[33] H. Dong, S.E. Paramonov, L. Aulisa, E.L. Bakota, J.D. Hartgerink, Self-assembly of multidomain peptides: balancing molecular frustration controls conformation and nanostructure, J. Am. Chem. Soc. 129 (41) (2007) 12468–12472.
[34] E.W. Fish, The reaction of the dental pulp to peripheral injury of the dentine, Proc. R. Soc. Lond. B. 108 (756) (1931) 196–208.
[35] Y. Zhao, X. Yuan, B. Liu, U.S. Tulu, J.A. Helms, Wnt-Responsive odontoblasts secrete new dentin after superficial tooth injury, J. Dent. Res. 97 (9) (2018) 1047–1054.
[36] O.A. Nada, R.M. El Backly, Stem cells from the apical papilla (SCAP) as a tool for endogenous tissue regeneration, Front. Bioeng. Biotechnol. 6 (2018) 103.
[37] R. Wigler, A.Y. Kaufman, S. Lin, N. Steinbock, H. Hazan-Molina, C.D. Torneck, Revascularization: a treatment for permanent teeth with necrotic pulp and incomplete root development, J. Endod. 39 (3) (2013) 319–326.
[38] L. He, J. Zhong, Q. Gong, S.G. Kim, S.J. Zeichner, L. Xiang, L. Ye, X. Zhou, J. Zheng, Y. Liu, C. Guan, B. Cheng, J. Ling, J.J. Mao, Treatment of necrotic teeth by apical revascularization: meta-analysis, Sci. Rep. 7 (1) (2017) 13941.
[39] G. Chen, J. Chen, B. Yang, L. Li, X. Luo, X. Zhang, L. Feng, Z. Jiang, M. Yu, W. Guo, W. Tian, Combination of aligned PLGA/Gelatin electrospun sheets, native dental pulp extracellular matrix and treated dentin matrix as substrates for tooth root regeneration, Biomaterials 52 (2015) 56–70.
[40] B. Chang, K.K.H. Svoboda, X. Liu, Cell polarization: from epithelial cells to odontoblasts, Eur. J. Cell Biol. 98 (1) (2019) 1–11.
[41] T. Gonzalez-Martinez, P. Perez-Pinera, B. Diaz-Esnal, J.A. Vega, S-100 proteins in the human peripheral nervous system, Microsc. Res. Tech. 60 (6) (2003) 633–638.
[42] T. Walchli, A. Wacker, K. Frei, L. Regli, M.E. Schwab, S.P. Hoerstrup, H. Gerhardt, B. Engelhardt, Wiring the vascular network with neural cues: a CNS perspective, Neuron 87 (2) (2015) 271–296.
[43] C. Zhan, M. Huang, X. Yang, J. Hou, Dental nerves: a neglected mediator of pulpitis, Int. Endod. J. 54 (1) (2021) 85–99.
[44] H. Zhao, J. Feng, K. Seidel, S. Shi, O. Klein, P. Sharpe, Y. Chai, Secretion of shh by a neurovascular bundle niche supports mesenchymal stem cell homeostasis in the adult mouse incisor, Cell Stem Cell 14 (2) (2014) 160–173.
[45] N. Kaukua, M.K. Shahidi, C. Konstantinidou, V. Dyachuk, M. Kaucka, A. Furlan, Z. An, L. Wang, I. Hultman, L. Ahrlund-Richter, H. Blom, H. Brismar, N.A. Lopes, V. Pachnis, U. Suter, H. Clevers, I. Thesleff, P. Sharpe, P. Ernfors, K. Fried, I. Adameyko, Glial origin of mesenchymal stem cells in a tooth model system, Nature 513 (7519) (2014) 551–554.
[46] J. Pizzicannella, S.D. Pierdomenico, A. Piattelli, G. Varvara, L. Fonticoli, O. Trubiani, F. Diomede, 3D Human periodontal stem cells and endothelial cells promote bone development in bovine pericardium-based tissue biomaterial, Materials (Basel) 12 (13) (2019).
[47] G.T. Huang, S. Gronthos, S. Shi, Mesenchymal stem cells derived from dental tissues vs. those from other sources: their biology and role in regenerative medicine, J. Dent. Res. 88 (9) (2009) 792–806.
[48] L. He, J. Zhou, M. Chen, C.S. Lin, S.G. Kim, Y. Zhou, L. Xiang, M. Xie, H. Bai, H. Yao, C. Shi, P.G. Coelho, T.G. Bromage, B. Hu, N. Tovar, L. Witek, J. Wu, K. Chen, W. Gu, J. Zheng, T.J. Sheu, J. Zhong, J. Wen, Y. Niu, B. Cheng, Q. Gong, D.M. Owens, M. Stanislauskas, J. Pei, G. Chotkowski, S. Wang, G. Yang, D.J. Zegarelli, X. Shi, M. Finkel, W. Zhang, J. Li, J. Cheng, D.P. Tarnow, X. Zhou, Z. Wang, X. Jiang, A. Romanov, D.W. Rowe, S. Wang, L. Ye, J. Ling, J. Mao, Parenchymal and stromal tissue regeneration of tooth organ by pivotal signals reinstated in decellularized matrix, Nat. Mater. 18 (6) (2019) 627–637.
[49] V. Rosa, Z. Zhang, R.H. Grande, J.E. Nor, Dental pulp tissue engineering in full-length human root canals, J. Dent. Res. 92 (11) (2013) 970–975.
[50] C.C. Huang, R. Narayanan, S. Alapati, S. Ravindran, Exosomes as biomimetic tools for stem cell differentiation: applications in dental pulp tissue regeneration, Biomaterials 111 (2016) 103–115.
[51] X. Li, C. Ma, X. Xie, H. Sun, X. Liu, Pulp regeneration in a full-length human tooth root using a hierarchical nanofibrous microsphere system, Acta Biomater. 35 (2016) 57–67.
[52] C.C. Huang, R. Narayanan, N. Warshawsky, S. Ravindran, Dual ECM biomimetic scaffolds for dental pulp regenerative applications, Front. Physiol. 9 (2018) 495.
[53] Y. Itoh, J.I. Sasaki, M. Hashimoto, C. Katata, M. Hayashi, S. Imazato, Pulp regeneration by 3-dimensional dental pulp stem cell constructs, J. Dent. Res. 97 (10) (2018) 1137–1143.
[54] H. Chen, H. Fu, X. Wu, Y. Duan, S. Zhang, H. Hu, Y. Liao, T. Wang, Y. Yang, G. Chen, Z. Li, W. Tian, Regeneration of pulpo-dentinal-like complex by a group of unique multipotent CD24a(+) stem cells, Sci. Adv. 6 (15) (2020) eaay1514.
[55] S.E. Millar, A pulpy story, Nat. Mater. 18 (6) (2019) 530–531.
[56] C.Y. Moon, O.H. Nam, M. Kim, H.S. Lee, S.N. Kaushik, D.A. Cruz Walma, H.W. Jun, K. Cheon, S.C. Choi, Effects of the nitric oxide releasing biomimetic nanomatrix gel on pulp-dentin regeneration: pilot study, PLoS One 13 (10) (2018) e0205534.
[57] L. He, S.G. Kim, Q. Gong, J. Zhong, S. Wang, X. Zhou, L. Ye, J. Ling, J.J. Mao, Regenerative endodontics for adult patients, J. Endod. 43 (9S) (2017) S57–S64.
[58] I. Fagogeni, J. Metlerska, M. Lipski, T. Falgowski, G. Maciej, A. Nowicka, Materials used in regenerative endodontic procedures and their impact on tooth discoloration, J. Oral Sci. 61 (3) (2019) 379–385.
[59] C. Jung, S. Kim, T. Sun, Y.B. Cho, M. Song, Pulp-dentin regeneration: current approaches and challenges, J. Tissue Eng. 10 (2019) 2041731418819263.
[60] S. Kim, S.J. Shin, Y. Song, E. Kim, In vivo experiments with dental pulp stem cells for pulp-dentin complex regeneration, Mediators Inflamm. 2015 (2015) 409347.
[61] K. Iohara, K. Imabayashi, R. Ishizaka, A. Watanabe, J. Nabekura, M. Ito, K. Matsushita, H. Nakamura, M. Nakashima, Complete pulp regeneration after pulpectomy by transplantation of CD105+ stem cells with stromal cell-derived factor-1, Tissue Eng. Part A 17 (15–16) (2011) 1911–1920.
[62] R. Ishizaka, K. Iohara, M. Murakami, O. Fukuta, M. Nakashima, Regeneration of dental pulp following pulpectomy by fractionated stem/progenitor cells from bone marrow and adipose tissue, Biomaterials 33 (7) (2012) 2109–2118.
[63] K. Iohara, M. Murakami, N. Takeuchi, Y. Osako, M. Ito, R. Ishizaka, S. Utunomiya, H. Nakamura, K. Matsushita, M. Nakashima, A novel combinatorial therapy with pulp stem cells and granulocyte colony-stimulating factor for total pulp regeneration, Stem Cells Transl. Med. 2 (7) (2013) 521–533.
[64] Y. Wang, Y. Zhao, W. Jia, J. Yang, L. Ge, Preliminary study on dental pulp stem cell-mediated pulp regeneration in canine immature permanent teeth, J. Endod. 39 (2) (2013) 195–201.
[65] J.W. Yang, Y.F. Zhang, C.Y. Wan, Z.Y. Sun, S. Nie, S.J. Jian, L. Zhang, G.T. Song, Z. Chen, Autophagy in SDF-1alpha-mediated DPSC migration and pulp regeneration, Biomaterials 44 (2015) 11–23.
[66] P.R. Arany, A. Cho, T.D. Hunt, G. Sidhu, K. Shin, E. Hahm, G.X. Huang, J. Weaver, A.C. Chen, B.L. Padwa, M.R. Hamblin, M.H. Barcellos-Hoff, A.B. Kulkarni, J.M. D, Photoactivation of endogenous latent transforming growth factor-beta1 directs dental stem cell differentiation for regeneration, Sci. Transl. Med. 6 (238) (2014) 238ra69.
[67] K.H. Vining, J.C. Scherba, A.M. Bever, M.R. Alexander, A.D. Celiz, D.J. Mooney, Synthetic light-curable polymeric materials provide a supportive niche for dental pulp stem cells, Adv. Mater. 30 (4) (2018).

[68] X. Luo, B. Yang, L. Sheng, J. Chen, H. Li, L. Xie, G. Chen, M. Yu, W. Guo, W. Tian, CAD based design sensitivity analysis and shape optimization of scaffolds for bio-root regeneration in swine, Biomaterials 57 (2015) 59–72.
[69] M. Yadlapati, C. Biguetti, F. Cavalla, F. Nieves, C. Bessey, P. Bohluli, G.P. Garlet, A. Letra, W.D. Fakhouri, R.M. Silva, Characterization of a vascular endothelial growth factor-loaded bioresorbable delivery system for pulp regeneration, J. Endod. 43 (1) (2017) 77–83.
[70] R. Langer, J.P. Vacanti, Tissue engineering, Science 260 (5110) (1993) 920–926.
[71] D.P. Kavanagh, N. Kalia, Hematopoietic stem cell homing to injured tissues, Stem Cell Rev. Rep. 7 (3) (2011) 672–682.
[72] V.A. Kumar, N.L. Taylor, S. Shi, N.C. Wickremasinghe, R.N. D'Souza, J.D. Hartgerink, Self-assembling multidomain peptides tailor biological responses through biphasic release, Biomaterials 52 (2015) 71–78.
[73] J. Zhang, H. Chen, M. Zhao, G. Liu, J. Wu, 2D nanomaterials for tissue engineering application, Nano Res. 13 (8) (2020) 2019–2034.
[74] X. Gao, Z. Xu, G. Liu, J. Wu, Polyphenols as a versatile component in tissue engineering, Acta Biomater. 119 (2021) 57–74.